Experimental and theoretical study of the properties of plasma containing a hemispherically focused ion beam

J. M. Peterson[a] and N. L. Oleson[b]
Department of Physics, University of South Florida, Tampa, Florida 33620

(Received 16 May 1990; accepted 3 January 1992)

Argon plasmas were produced in a modified multipole plasma device in which the electrons in the two plasmas were isolated by a *hemispherical* center grid biased negatively. Whenever ion beams are caused to stream from the driver plasma into the target plasma, an additional cold group of Maxwellian electrons were observed in the target plasma. The objective of this paper is to explore the properties of this double-beam plasma (DP) device. Hopefully, this information would provide a reason for the appearance of the cold electron group. To this end, measurements were made of the ion beam densities, energies, and ion temperatures at various axial distances from the hemispheric's separating grid. Similarly, movable Langmuir probes and hot emissive probes were used to measure the corresponding electron temperatures, densities, and plasma potentials. All that can be said is that these data would suggest that the additional cold group of electrons could result from the interaction of the ion beam with the target electrons in the path of the ion beam. These cold electrons appear to ride along with the ion beam since they are detected throughout the target plasma, since the cold group of electrons are found everywhere in the target plasma.

I. INTRODUCTION

The main objective of this paper is to call attention to some low-energy ion beam research and its connection to what was formerly called gaseous electronics in the 1930s and 1940s. This almost classical investigation has resulted in the observation of a low-energy group of electrons in a plasma that contains a focal point. In addition, we illustrate the kind of diagnostic equipment used in this type of investigation. Finally, we shall express some thoughts on the possible origin of low-energy groups of electrons.

A significant breakthrough took place in the early seventies in ion beam technology by the development of the multidipole double-beam plasma device (DP) by Taylor *et al.*[1] It consists of two independent plasmas, the driver plasma, and the target plasma, which are separated from each other by a dividing screen. The plasmas can be operated at the same potential or different potentials, the dividing screen being biased negatively to prevent electrons from moving from the driver to the target plasma. If the driver plasma is maintained at a higher potential than that of the target plasma, an ion beam penetrates the target region, its magnitude being controlled by the driver plasma. The magnetic multipole field boundaries containing the plasma were configured by placing ceramic bar magnets parallel to each other and running along the inside walls of the cylindrical plasma device, with alternating north and south polarities. Such an arrangement provides a magnetic field close to the wall boundaries that reflects energetic electrons, and thus prevents their excessive loss to ground[1] (see Fig. 1). This device has proven to be a boon for the production of plasmas of greater charge densities and for the study of the interaction of ion pulses and beams with plasmas, and is evidenced by the list of references provided in a paper of Honzawa.[2] These references include papers making use of DP's having plane, cylindrical, and spherical separating screens. If the two plasmas are kept at the same potential (no beam) and a small positive pulse applied to the driver anode (or the separating screen), an ion acoustic wave is detected in the target plasma. Increasing the pulse amplitude results in the formation of ion acoustic solitons in the target plasma. These solitons (a form of solitary wave) are referred to as plane, cylindrical, or spherical, corresponding to the geometrical shapes of the dividing screens. Each type has distinct properties. Recently, a paper has appeared in which a DP device is used where the separating screen is hemispherical and where the generated solitons have different properties from those of spherical solitons.[3] Their collisional properties are the same, however, when two solitons are moving in the same direction.

If the driver plasma is maintained at a higher voltage than the test plasma, an ion beam flows from the driver plasma to the test plasma. If now, in addition, a small pulse or a continuous wave is superimposed on the voltage of the driver, the so-called ion beam modes also appear in the test plasma as well as the ion acoustic wave.

More recent publications using conventional DP's for the study of solitons and ion beam modes are given in Refs. 2 and 4–9. This list provides support for the statement made previously about the importance of the DP device. Consequently, it is desirable to know more about the properties of the double plasma device in the present case, where the dividing screen is hemispherical in shape and a focal point

[a] Present address: Department of Transportation, Juneau, Alaska.
[b] Present address: The Department of Electrical Engineering, Box 118, University of South Florida, Tampa, Florida 33620.

 0899-8221/92/040888-14$04.00

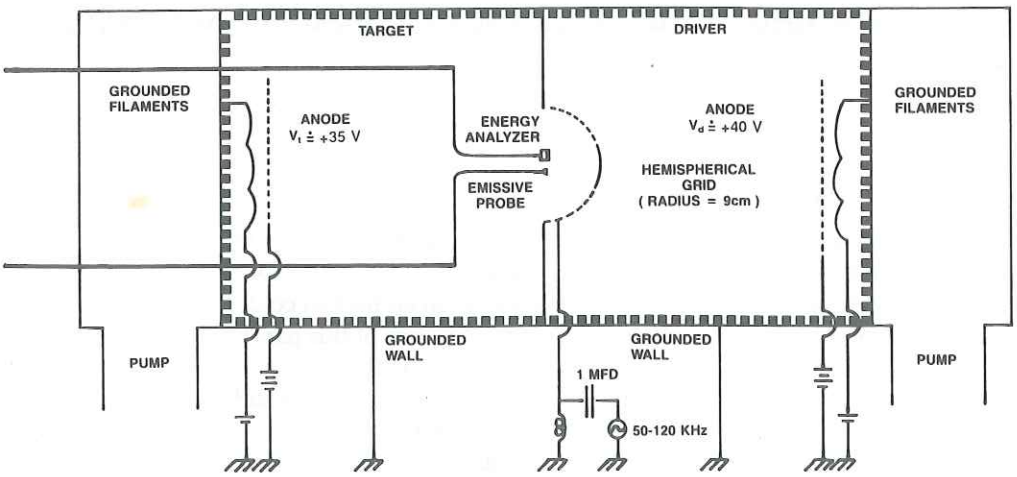

FIG. 1. Multipole double-plasma device. Ceramic magnets are indicated by ■■■... and represent bar magnets parallel to each other and running along the inside walls of the plasma device with alternating north and south polarities.

appears in the test plasma and is more experimentally accessible than one containing a spherical dividing screen.

This paper is arranged as follows: Sec. II discusses experimental details; Sec. III describes the diagnostics used; Sec. IV gives a brief discussion of the linear theory of ion beam modes when the dividing screen is spherical (no theory exists for a hemispherical dividing screen); Sec. V is concerned with experimental formulas and observations, being divided into four parts [(a) relative beam density, (b) beam velocity, (c) Langmuir plots, and (d) discussion of low temperature electrons]; Sec. VI gives summary and conclusions; Appendix A is concerned with cold and hotter ions; and Appendix B gives a method of obtaining the relative charge density at the focus.

II. EXPERIMENT

Figure 1 is the DP device that was constructed in our laboratory. The apparatus was pumped down to 10^{-6} Torr and then filled with argon to a pressure of 0.4 mT. The anode screen in each plasma was located directly in front of the filaments rather than at the walls. Each anode determined the potential of the adjacent plasma so that the potential at each point was close to the anode potential, as corroborated by Langmuir probe measurements. In most cases, the driver anode voltage was kept fixed at 45 V while the target anode voltage was varied from 45 to 30 V or less. This was done to vary the energy of the ion beam passing from the driver plasma to the target plasma, a well-known technique. All voltages were with respect to the grounded stainless steel cylindrical container. Because of this, the most energetic electron group was reflected back into the plasma by the magnetic cusps formed by the ceramic bars at the walls. At the same time, the loss of positive ions to the walls was greatly reduced via ambipolar diffusion with the slower and thermal electrons.[10,11] One consequence of this was the lack of need to insulate the grounded metal probe supporting rods to prevent sparking. The cylindrical vessel was of stainless steel 50 cm in diameter and 150 cm long. The chosen electron concentration and electron temperature were such to give a Debye length of approximately 0.64 mm, much greater than the distances between dividing screen elements. This ensured the effectiveness of the electric field of the screen in preventing passage of electrons from the driver to the target plasma. At the same time, the small magnitude of the Debye length allows us to make the assumption that the sheath formed at the dividing screen had little effect upon the hemispherical focusing of the grid. This allows us to say that the grid and the sheath around the grid form concentric hemispheres differing in radius by only a few Debye lengths.

The velocities of ion waves, beam ions, and thermal ions were much smaller than those of the electrons, and the latter was treated as a neutralizing negative fluid.

III. DIAGNOSTICS

All probes were mounted on a movable probe assembly designed by Mattson.[12] Spherical Langmuir probes were constructed in accordance with a method described by Garner.[13] These probes were used for wave detection and Langmuir plots because the spherical probe is known to minimize the distortion of the probe characteristics in the presence of directional motion.[14]

An emissive probe with rapid scanning and slow scanning circuits was built according to the specifications of Smith *et al.*[15] It is essentially a hot tungsten wire probe heated sufficiently to allow thermionic emission of electrons and biased with respect to space potential. When the applied voltage V_g was positive with respect to space potential, the emitted electrons were drawn back to the probe and the collected electron current was essentially unaffected by the emission. On the other hand, when the probe was negative with respect to the space potential, the emitted electrons escaped and contributed an apparent ion current to the probe. Thus the voltage at which the hot and cold probe characteristics disagree correspond closely to the space potential. Figure 2 shows both cold and hot curves taken at the focus in the presence of an ion beam resulting from a difference of potential of 10 V between the driver anode and the target anode. Note that the cold probe curve shows a little indication of a "break point" at plasma potential V_p. When the emissive probe was heated up to emission, however, the characteristic curves were almost identical for $V_g > V_p$ such that the floating potential of the hot probe approached the true plasma potential V_p, as

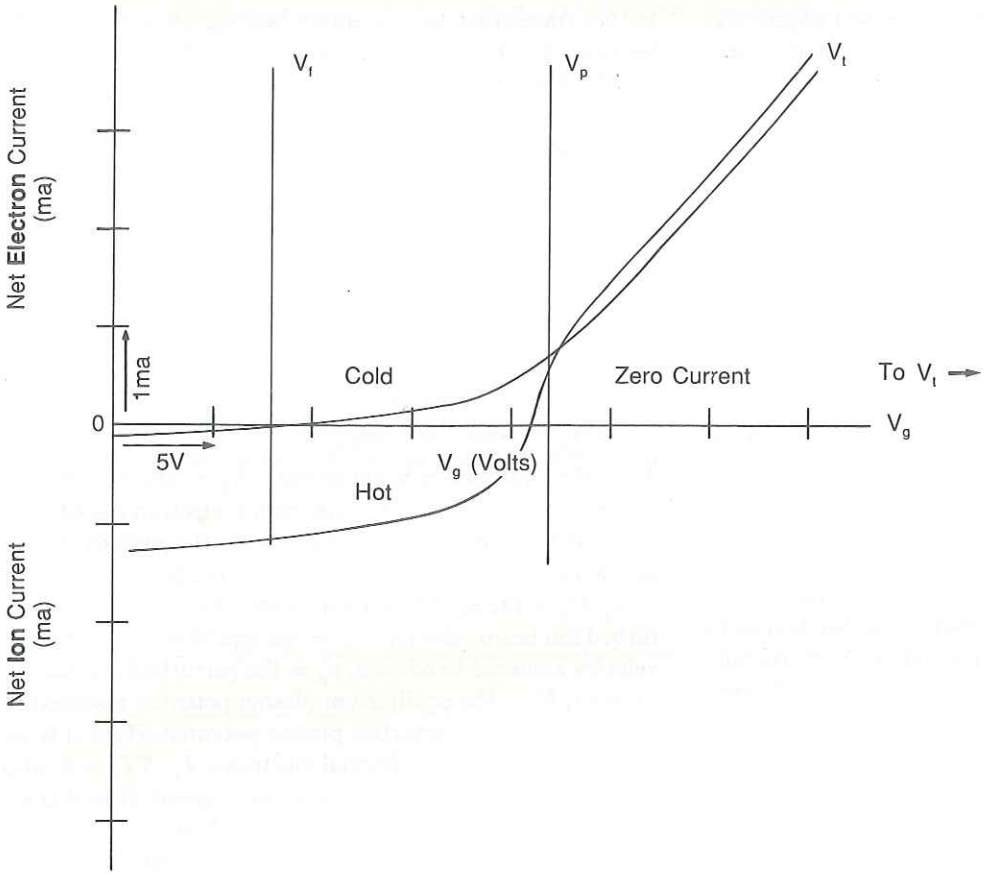

FIG. 2. Cold and hot probes: probe current i_p versus applied bias voltage V_g. Here, V_p is the plasma potential determined by the inflection point method.[15] Ion beam energy is $V_b = 10$ V.

determined by the inflection point method[15] to within 1.0 V. This provided a simple method for monitoring the plasma potential at any point within the target plasma when an ion beam is present.

Figure 3 is a plot of the floating potential (zero probe current) along the axis of the target plasma for different degrees of emission for an ion beam of 10 V energy. The curve for saturated emission indicates that the plasma potential remained constant throughout the plasma and was within 1 V of the anode potential. The curve for no emission, however, indicated a change in floating potential near the target focus. This peculiar behavior will be discussed later in connection with the electron temperature.

A modified Ikezi–Taylor electrostatic double grid ion energy analyzer was constructed in our laboratory to monitor the ion energy distribution[16] (Fig. 4). The outer grid was allowed to float and so to retard most of the electrons and to minimize the disturbance of the plasma by the energy analyzer. The second (inner) grid was biased positively to retard the ions and was used for energy selection of the ions.

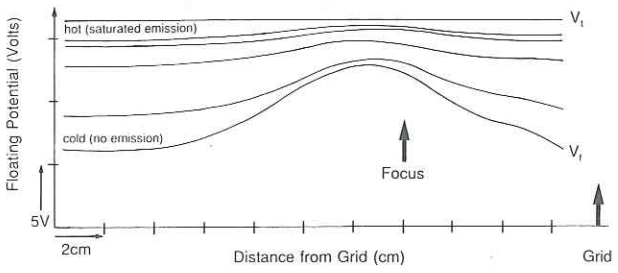

FIG. 3. Plots of the floating potential of the emissive probe along axis of plasma for different degrees of emission. Here, V_t is the target anode potential. Ion beam energy is $V_b = 10$ V.

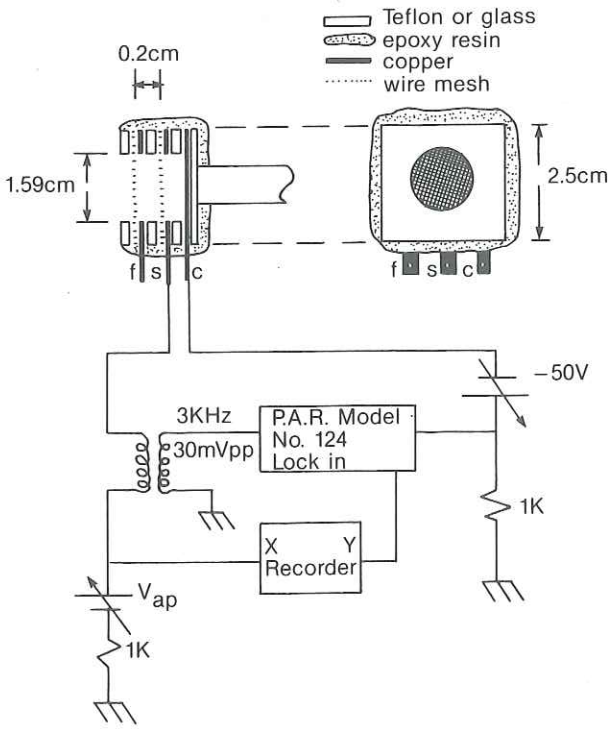

FIG. 4. The ion energy analyzer with differentiating circuit. *f*: floating grid; *S*: selector grid; *C*: collector plate; V_{ap}: selector grid voltage.

The collector plate, which was originally biased negatively, typically -50 V, repelled the residual high-energy electrons that may have gotten through the outer grid so that only the ion current was collected.

As previously noted, in order for the inner grid to have a well-defined separating action, the electric field on the wires must extend over the areas of the holes; or the dimensions of the holes must be small compared to the Debye length. An electron micrograph of the copper mesh used for the inner grid reveals a hole size of about 0.01 mm. This is much less than the Debye length ($L_D = 0.64$ mm). A stainless steel outer grid with a hole size of 0.2 mm $< L_D$ was used to repel most of the electrons.

Ion-current-voltage characteristics were obtained by plotting directly the current to the collector $I(V_{ap})$, as a function of the selector voltage V_{ap}. The relative beam density, the ratio of N_b to $N_b + N_p$, was determined from the relative saturation currents, as will be discussed later. Here, N_p is the plasma density and N_b is the ion beam density.

A plot of the ion velocity distribution perpendicular to the plane of the energy analyzer was obtained from ion-current-selector voltage characteristic curve by the following procedure:

$$I(V_{ap}) = enA \int_{u_{min}}^{\infty} uf(u)du, \tag{1}$$

where e is the electric charge on the ion, A is the effective mesh area, n is the ion density, $f(u)$ is the ion beam velocity distribution, and u is the component of ion velocity normal to the surface of the analyzer. The minimum velocity u_{min}, selected by the inner grid, is given by

$$m_i u_{min}^2 = \begin{cases} 2e(V_{ap} - V_p), & \text{for } V_{ap} > V_p, \\ 0, & \text{for } V_{ap} < V_p, \end{cases} \tag{2}$$

where V_p is the plasma potential. Differentiating the collector current in Eq. (1) with respect to the selector voltage V_{ap} yields

$$\frac{\partial I}{\partial V_{ap}} = \begin{cases} \propto f(u), & \text{for } V_{ap} > V_p, \\ 0, & \text{for } V_{ap} < V_p. \end{cases} \tag{3}$$

The electrical circuit shown in Fig. 4 was used to plot the differentiated ion characteristic using the following scheme: Through a transformer, a 3 kHz, 0.03 V peak-to-peak signal from the generator in the Princeton Applied Research Model (124) lock-in amplifier was put in series with the inner grid selector dc voltage V_{ap}. The ac current to the collector was measured by its corresponding voltage drop across the 1 kΩ resistor in series with V_{ap} in Fig. 4. That part of this voltage which was in phase with the transformer voltage was proportional to $\partial I(V_{ap})/\partial V_{ap}$. The lock-in amplifier was adjusted to measure the in-phase part, which was plotted as a function of V_{ap}, simply displaying $f(u)$ in units of arbitrary amplitude. The results of these measurements will be discussed in the following sections.

IV. ION BEAM MODES

The following discussion of ion beam mode analysis is relevant since DP devices are frequently used to study ion beam modes and solitons. The properties of the plasma that we are measuring have a direct bearing on the ion mode behavior. Garner[13] used the linear theory of ion beam modes in spherical geometry in an attempt to interpret the experimental results for the hemispherical case. The basic linearized equations are as follows:

$$\frac{\partial n_b}{\partial t} + \nabla\cdot(n_b U_b) = 0, \tag{4a}$$

$$\frac{\partial u_b}{\partial t} + U_b\cdot\nabla u_b + \frac{e}{M_i}\nabla v_{p_1} = 0, \tag{4b}$$

$$n_e = N_e \exp\left(\frac{ev_{p_1}}{KT_e}\right), \tag{4c}$$

$$\nabla^2 v_{p_1} = 4\pi e n_e - 4\pi e n_b, \tag{4d}$$

N_b = the equilibrium beam density, N_p = the equilibrium plasma density, N_e = the equilibrium electron density, n_b = the perturbed ion beam density, n_p = the perturbed plasma density, n_e = the perturbed electron density, $n_e = n_b + n_p$, U_b = the equilibrium ion beam velocity, u_b = the perturbed ion beam velocity, U_p = the equilibrium plasma ion velocity assumed to be zero, u_p = the perturbed plasma ion velocity, V_p = the equilibrium plasma potential assumed to be zero, v_{p_1} = the perturbed plasma potential. Here, it is assumed: cold ions, hot thermal electrons, T_e, $\nabla T_e = 0$, and $U_b/C_s > 1$, where C_s is the ion acoustic speed. It is also assumed that the plasma ions are fixed so that $n_p = 0$.

The steady-state solutions for the above set of equations revealed that $r^2 n_b U_b$ was constant, where r was the distance from the focus (a singular point). Solving the above set of equations allowed elimination of the perturbed velocity u_b. Making use of the normal mode approach gave the phase velocity C_p of fast and slow modes, the + and − signs refer to the fast and slow modes, respectively:

$$C_{p\pm} = w/k = U_b \pm B^{1/2} C_s, \tag{5}$$

where C_s is the ion acoustic speed in the test plasma. The perturbed density of those modes is found from

$$\frac{r\,\partial n_b}{n_b\,\partial r} = -\frac{2(1 \pm B)^{3/2} U_b^2}{C_s C_{p\pm}}, \tag{6}$$

where B is the relative beam density given by

$$B = N_b/(N_b + N_p) \tag{7}$$

and r is the distance from the focal point. Integration of Eq. (6) and use of Eq. (5) give

$$n_b \sim r^{K_f s}, \tag{8}$$

$$K_f = -2\left(\frac{1 + [N_b/(N_p + N_b)]^{3/2}(C_s/V_b)}{1 + [N_b/(N_p + N_b)]^{1/2}(C_s/V_b)}\right)$$

fast mode, (9)

$$K_s = -2\left(\frac{1 - [N_b/(N_p + N_b)]^{3/2}(C_s/V_b)}{1 - [N_b/(N_p + N_b)]^{1/2}(C_s/V_b)}\right)$$

slow mode. (10)

The amplitudes of these modes increase as the focal point is approached. This is in contrast to the $1/r^2$ relations obtained from geometrical consideration. It is seen that the ampli-

tudes of the fast and slow modes do not vary as $1/r^2$ but a fraction of the exponent -2.

Since the dividing screen is hemispherical in shape, the behavior of the beam far beyond the focal point should be similar to that of a flat screen and the problem is no longer a spherically symmetric one. Consequently, one would expect the ion density along the axis of the target plasma would increase as the focal region is approached from the screen, then followed by a decrease beyond this region, finally reaching constant value for large distances from the screen. Experimentally, Garner found that, for the fast beam mode (the predominant mode in the present case), the amplitude increased to maximum in the neighborhood of the focal point, then gradually decreased in magnitude beyond that point.[13] The phase velocity of the fast mode behaved in a similar fashion. Consequently, one must contend with the presence of these waves as well. The phase velocities and the perturbed densities of the ion beam mode are seen to be critically dependent on the properties of the beam velocity U_b, B and the magnitude of C_s, the ion acoustic speed, which is proportional to $T_e^{1/2}$.

Accordingly, U_b and B were monitored with the double-gridded ion-energy analyzer, while the electron temperature was carefully determined from the Langmuir probe plots. These topics are discussed further in the next section.

V. EXPERIMENTAL FORMULAS AND OBSERVATIONS

A. The determination of the relative beam density B

Figure 5 shows a series of ion current characteristic curves of the ion current reaching the collector electrode of

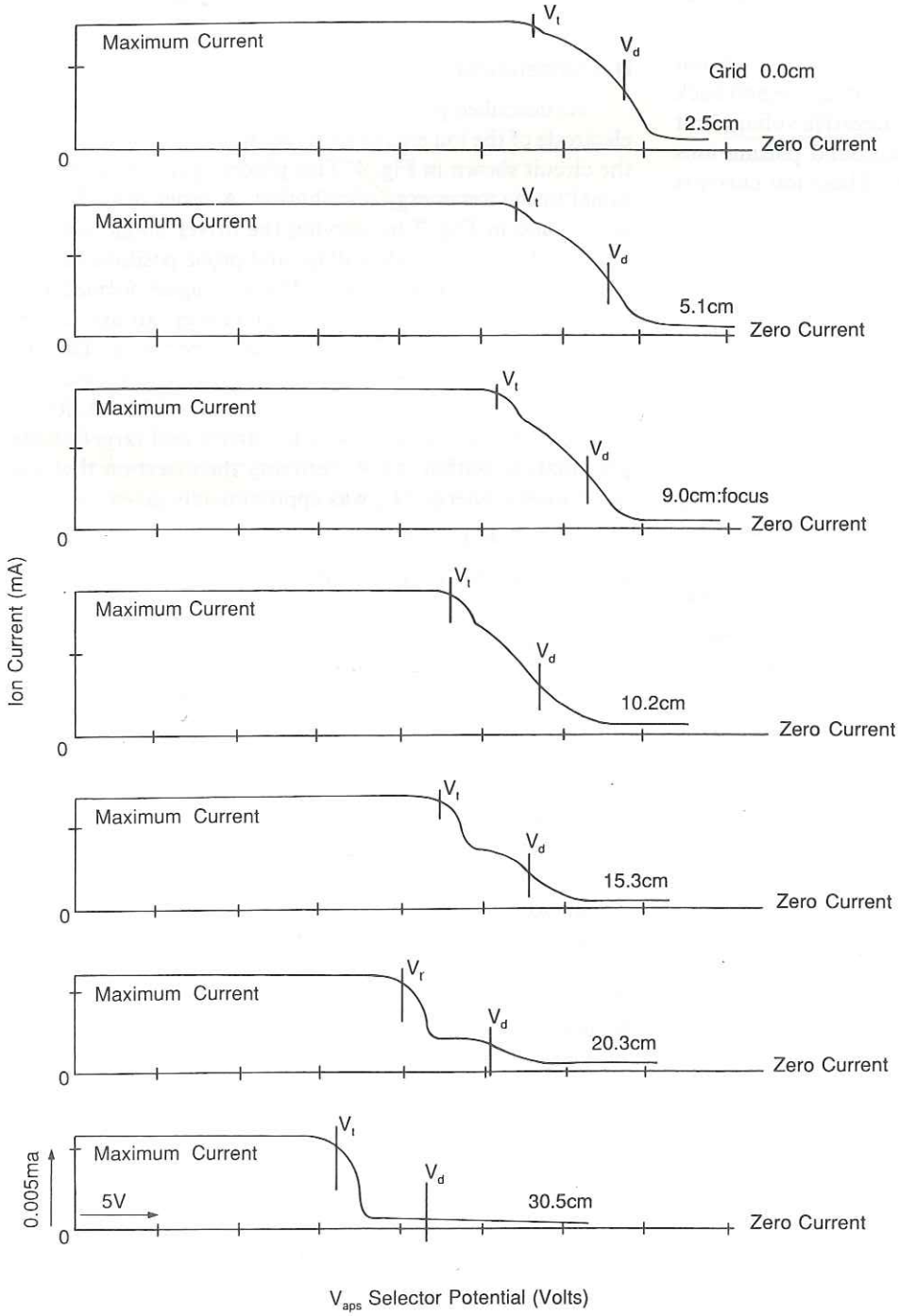

FIG. 5. Ion current reaching the collector electrode of the energy analyzer as a function of selector grid voltage V_{ap} for different probe positions. Probe position is in cm from hemispherical grid. All plots were made for a given beam energy: $eV_b \doteq eV_d - V_t) = 5.1$ eV. Here, V_d and V_f were held constant throughout the run. For reference, vertical lines were drawn across each plot: one each for the values of V_d and V_t. See Sec. II for further explanation.

the energy analyzer as a function of selector grid voltage V_{ap}. The vertical lines marked on each curve are the anode potentials of the target and driver plasmas, which are found from emissive probe measurements, the usual methods when charged beams are present. The curves not too far beyond the focus clearly shows two distinct groups of ions: the low-energy group, which are cut off near the target anode voltage, constitutes the ions in the background having density equal to N_p; the high-energy ions, which are cut off near the driver anode voltage, correspond to the differences in driver and target anode voltages having a density N_b.

In order to derive the relative beam density from these curves, the relative beam current must first be distinguished. Figure 6 is the curve in Fig. 5 taken 20 cm from the grid or 11 cm beyond the focus, where the beam is easily distinguished. (This would not be true for greater distances such as 30.5 cm from the screen where the ion beam density becomes very small because of its divergence.) The ion beam saturation current is extrapolated from the positive energy region back to a negative voltage as shown. At this negative voltage, not only the beam ions, but also the background plasma ions have reached their saturation currents. These ion currents are

$$i_b = N_b e u_b, \tag{11}$$

$$i_p = N_p e u_p, \tag{12}$$

where

$$m_i u_b^2 = \begin{cases} 2e(V_b - V_{ap}), & \text{for } V_b > V_{ap}, \\ 0, & \text{for } V_b < V_{ap}, \end{cases} \tag{13a}$$

$$m_i u_p^2 = \begin{cases} 2e(V_p - V_{ap}), & \text{for } V_p > V_{ap}, \\ 0, & \text{for } V_p < V_{ap}, \end{cases} \tag{13b}$$

$V_p \doteq V_t$, is the plasma potential, in the target plasma.

The average kinetic energy of a beam ion is

$$eV_b \doteq e(V_d - V_t), \tag{14}$$

and V_{ap} is the applied selector grid bias voltage in the energy analyzer. The relative beam density is, therefore, using Eqs. (7), (11), and (12), given by

$$B = \{1 + (i_p/i_b)[(V_b - V_{ap})/(V_p - V_{ap})]^{1/2}\}^{-1}. \tag{15}$$

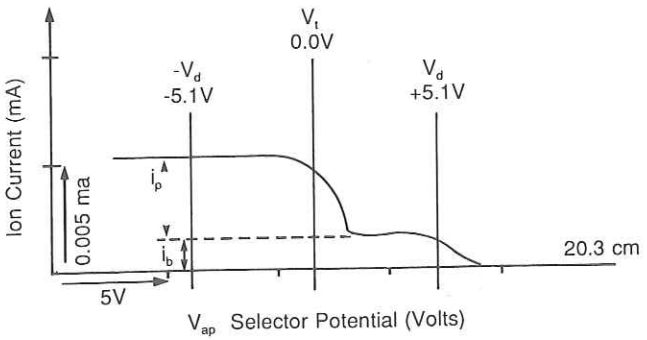

FIG. 6. The ion beam saturation current extrapolated from the positive to the negative energy region to determine the ratio i_p/i_b. The voltage values have been rescaled from those of Fig. 5 in the interest of clarity.

If we chose V_{ap} such that $(V_b - V_{ap})/(V_p - V_{ap}) = 2$, then

$$B = [1 + (i_p/i_b)2^{1/2}]^{-1}. \tag{16}$$

The task of determining B then reduces to "guessing" how much ion current is due to the ion beam and how much is due to the background plasma on the target side. This guessing process is indicated by the dotted line in Fig. 6. It was drawn parallel to the horizontal axis, which seemed to make sense because of the shape of the characteristic curve in that figure. From Fig. 6, $i_p/i_b = 3$ at the required V_{ap}, and therefore $B = 0.19$ at a position 11 cm beyond the focus. A similar calculation showed that B is as high as $\frac{18}{19} \cong 1$ at the focus (see Appendix B). As can be seen, the undifferentiated ion current characteristic was used above to approximate a value for B in terms of the two saturated currents i_b and i_p.

B. The behavior of the beam velocity U_b

As described previously, the ion current to the collector electrode of the ion energy analyzer was differentiated using the circuit shown in Fig. 4. This process gave plots proportional to the ion energy distribution. A series of such plots were made in Fig. 7 by varying the driver anode voltage, holding the target anode voltage and probe position (11 cm beyond the focus) both fixed. The ions again formed two distinct groups: the low- and high-energy groups corresponding to the target and beam ions, respectively. The difference in energy between the two groups was a measure of the average kinetic energy of a beam particle. This was found to be equal to the difference in the driver and target anode potentials to within 0.5 V, verifying the assertion that the beam kinetic energy eV_b was approximately given by

$$e(V_d - V_t) = eV_b, \tag{17}$$

where V_d, V_t are the driver and target anode voltages, respectively.[15]

Great care must be used in interpreting the plots of Fig. 7, which are essentially plots of ion number densities versus ion energies if half-widths are used as an indication of the temperature, and the areas under the curves as an indication of number density. It is difficult to compare temperatures and densities of the higher- and lower-energy groups from an examination of Fig. 7. However, the beam ions have undergone an acceleration in passing through the hemispherically dividing screen into the target plasma, whereas the target plasma ions have not. In a similar experiment using a cylindrical separating screen between the driver and target plasmas, Romesser and Hershkowitz[17] also obtained a plot similar to the plots of Fig. 7. They found that, if the higher-energy group was replotted versus their velocity with respect to the lower energy target plasma ion group (average velocity equal to zero), the number density and temperature of the higher-energy group were found to be much less. This is the phenomenon of "cooling by acceleration," meaning that, if an ion beam is accelerated to the velocity U_b, it is adiabatically cooled to a temperature T_b, where $T_b/T_i < 1$. In a recent review article, Hershkowitz discussed this effect in some detail.[18] In our case, this cooling would presumably occur when the ions were accelerated as they passed through

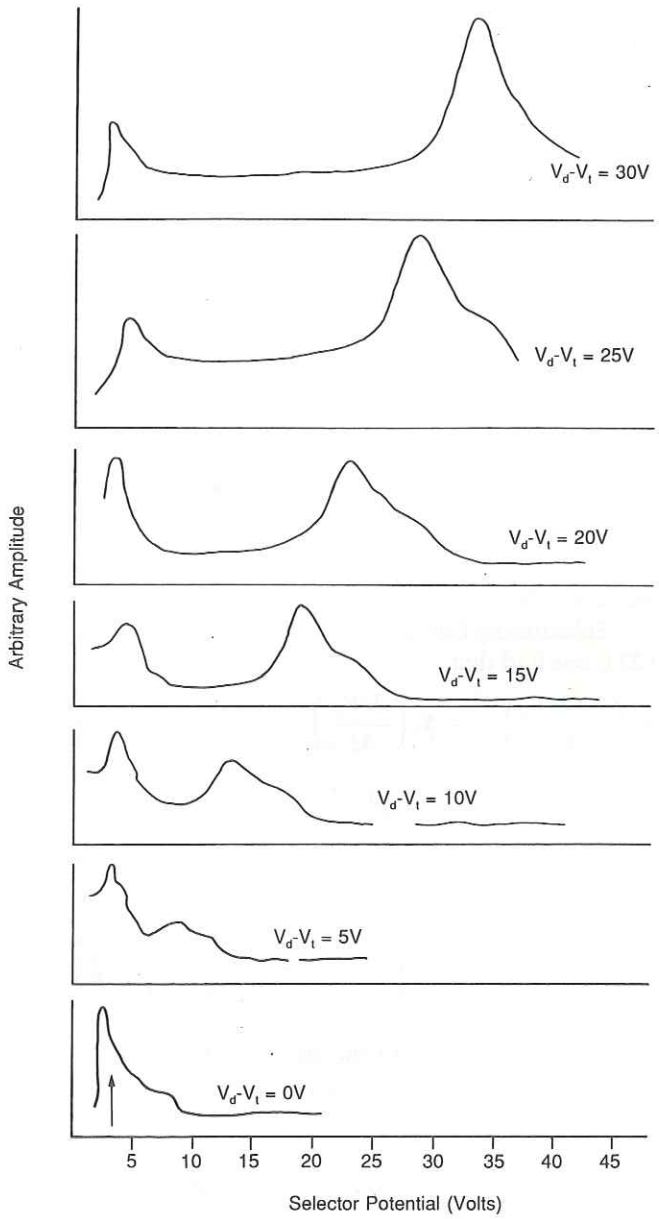

FIG. 7. Differentiated ion energy analyzer plots taken 11 cm beyond the focus for various values of $V_d - V_t$. The voltage difference between the two humps verified the relation $eV_b = e(V_d - V_t)$.

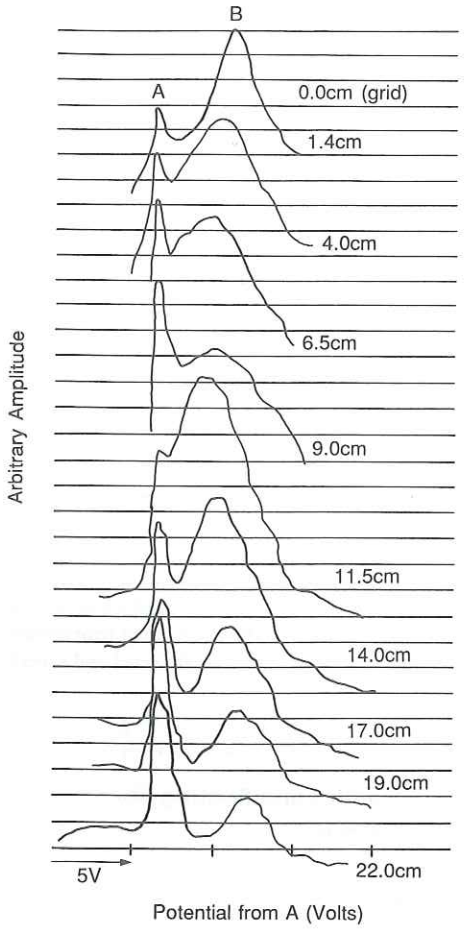

FIG. 8. Ion energy distribution for various positions. Here, $V_b = 8$ V. Here A corresponds to the background ions and B to the beam ions, respectively. As indicated, the vertical scale for each position is the same.

the hemispheric separating screen. Similar cooling effects have been observed in high-energy charged-particle accelerators.[19] Figure 8 shows the spatial evolution of $f(u)$ as the energy analyzer is moved from the hemispherical grid through and beyond the focus along the target plasma axis. For this set of data, the driver and target anodes were held at fixed voltages so that their difference was always 8 V. The hump corresponding to the target plasma occurred at a constant value of voltage close to the target plasma potential, whereas the beam hump seemed to decrease in energy as the analyzer passed through the focus but appeared to return to its original value again far beyond the focus. One is tempted to conclude that the beam ions slowed down as they approached the focus and speeded up as they left. One should bear in mind that the ion energy analyzer measures that portion of the ion energy whose velocity is perpendicular to the collector surface. The angle ϕ that the ion velocity makes with the normal to the collector surface depends not only on its position with respect to the focal point, but also on that portion of the hemispherical screen through which it passes in coming from the driver plasma. Consequently, it is necessary to average over ϕ as is done in obtaining Eq. (A1) in Appendix A. This equation is plotted as the solid line in Fig. 9 for a constant U_b, the average velocity ($V_b = 8$ V), and zero ion temperature. The experimental points (circle with a dot) in that figure were obtained by plotting the difference in energy between the background ions and the beam ions in Fig. 8.

The curve could produce a better fit to the experimental pointer when the anisotropy of the beam ions, because of their temperature as they enter the target plasmas, is considered [see Eq. (A2) in Appendix A]. We conclude that U_b was almost constant and that there existed only a very small potential gradient in the target plasma due to the ion beam.

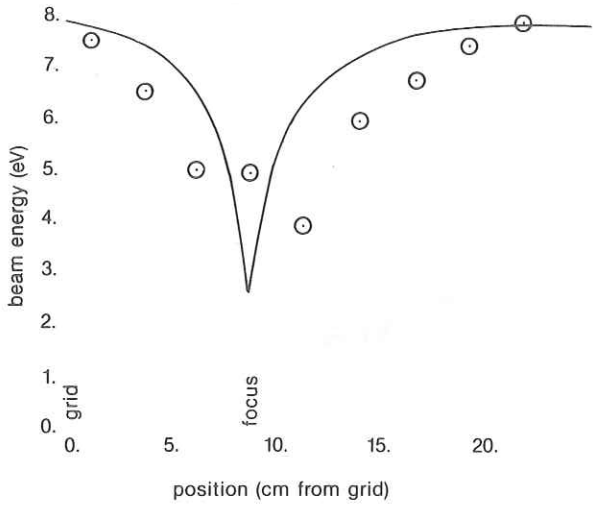

FIG. 9. Apparent average beam energy versus position; the solid curve is the calculated value [see Fig. (13)]. The experimental points were obtained from the differences in energy between background ions and the beam ions in Fig. 8, neglecting the ion temperature T_i. The effect of ion temperature may account for the large discrepancy between the calculated and experimental values at the focus.

C. Electron and ion dynamics and floating potential in the presence of an ion beam

The first attempt to develop a theory for ion and electron collection by a probe immersed in a plasma was done by Langmuir and Mott-Smith in 1926.[20] Their theory assumed a positive ion space charge sheath surrounding the probe into which only very high-energy electrons could penetrate and no ion beam was assumed to be present.

It is clear that the voltage of the sheath edge V_s must be large and negative enough to prevent a significant fraction of the plasma electrons from entering the sheath. Hence

$$-eV_s \cong KT_e, \tag{18}$$

where the plasma potential V_p is put equal to zero, and where it is assumed that the electrons have a Maxwell–Boltzmann distribution corresponding to a temperature T_e.

The electron current reaching the probe is found from the Boltzmann relation $n_e = N_0 \exp(eV_0/KT_e)$ and the fact that

$$I_e = -ea_p N_0 (KT_e/2\pi m_e)^{1/2} \exp(eV_0)/KT_e, \tag{19}$$

where V_0 is the potential of the probe (negative with respect to $V_p = 0$), N_0 is the unperturbed target plasma density, and a_p is the area of the probe.

If an ion beam is present in the target plasma, the ions entering the probe sheath are in two groups:

(1) The cold *background ions* with an average velocity equal to zero, which acquire a velocity at the sheath edge of

$$U_p = (-2eV_s/M_i)^{1/2}, \tag{20}$$

where N_p is the density of this group.

(2) The cold *beam ions* with average velocity

$$U_b = (2eV_b/M_i)^{1/2}, \tag{21}$$

where N_b is the density of this group and eV_b is the beam energy.

The total ion current to the probe, associated with the above two ion groups is

$$I_i = ea_s(N_p U_p + AN_b U_b), \tag{22}$$

where, as before, a_s is area of the sheath and

$$N_0 = N_p + N_b.$$

But, $O < A < 1$ is the fraction of the probe surface facing the beam. The experimental studies in this section made use of a *plane* probe always facing the beam. Therefore A can be put equal to 1.

If now the probe is allowed to "float" such that the net current to the probe is zero, $I_e + I_i = 0$ and using Eqs. (19) and (22) one obtains

$$-ea_p N_0 (KT_e/2\pi m_e)^{1/2} \exp(eV_f/KT_e) + ea_p(N_p U_p + N_b U_b) = 0 \tag{23}$$

around the probe, since the Debye length was approximately 0.64 mm. Here, $V_0 \to V_f$, the floating potential, and $a_s \to a_p$ because of the small sheath thickness.

Substituting Eqs. (20) and (21) for U_p and U_b into Eq. (23), one find that

$$N_p\left(\frac{-2eV_s}{M_i}\right)^{1/2} + N_b\left(\frac{2eV_b}{M_i}\right)^{1/2} = N_0\left(\frac{KT_e}{2\pi m_e}\right)^{1/2} \exp\left(\frac{eV_f}{KT_e}\right). \tag{24}$$

Making use of Eq. (18) and $B = N_b/N_0$, and taking the logarithm of both sides,

$$-\frac{1}{2}ln\left(\frac{M_i}{4\pi m_e}\right) + ln\left[1 - B + B\left(\frac{eV_b}{KT_e}\right)^{1/2}\right] = \frac{eV_f}{KT_e}. \tag{25}$$

For no beam, $B = 0$ and the above relation reduces to the usual case relating the floating potential to the electron temperature and becomes the well known result

$$\frac{eV_f}{KT_e} = -\frac{1}{2}ln\left(\frac{M_i}{4\pi m_e}\right) = -4.3 \text{ for argon.} \tag{26a}$$

Equation (25) becomes, for argon plasma containing an ion beam,

$$\frac{eV_f}{KT_e} = -4.3 + ln\left[1 - B + B\left(\frac{eV_b}{KT_e}\right)^{1/2}\right]. \tag{26b}$$

When a beam is present $0 < B < 1$, and the second term in the right-hand side of the above equation indicates two regions of interest: (a) when ratio $eV_b/KT_e < 1$, and (b) when ratio $eV_b/KT_e > 1$.

Assuming, for the sake of discussion, that $eV_b/KT_e = \text{const}$, then in case (a), as the probe is moved into regions of high B, the second term on the right becomes *negative*. The effect is to lower the floating potential at the focus. On the other hand, when case (b) is reached (say by increasing the beam energy eV_b), the second term on the right becomes more *positive* in regions of high B, resulting in an increase in the floating potential at the focus.

The transition from case (a) to case (b) occurs when $eV_b/KT_e > 1$. Experimentally, this transition is marked by a constant floating potential throughout the target plasma, even at the focus. From Fig. 10, this occurs when the beam

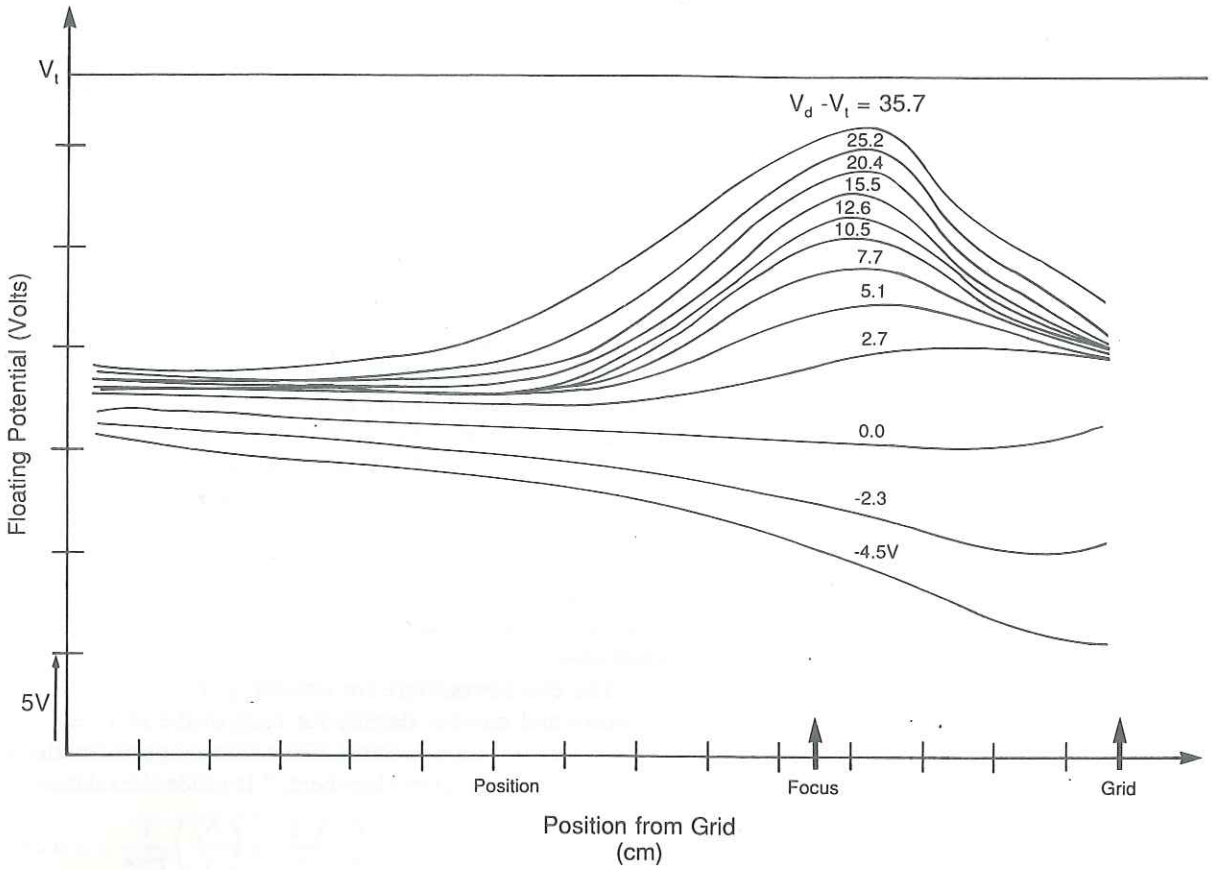

FIG. 10. The behavior of the floating potential V_f of a cold Langmuir plane probe along the axis for different beam energies. Floating potentials are determined by measuring the potential difference between the floating probe and the target anode as reference. Here, V_t is the target anode potential. Recall that the floating potential is negative with respect to V_t.

energy is between 0.0 and 2.7 eV.

The simple theory of this section was an attempt to explain the behavior of the floating potential of a probe in the presence of an ion beam. The theory revealed two kinds of behavior in agreement with the experiment (Fig. 10). The conclusion can be made then that it was the beam ions striking the probe that made its floating potential go up, or down, depending on the ratio eV_b/KT_e.

D. The Langmuir plots

As early as 1926, Langmuir and Mott-Smith[20] found, in the regions of intense ionization near the cathode, two superimposed Maxwellian distributions, one of relatively high mean energy, apparently consisting of primary electrons from the cathode, which have been scattered, and the other of much lower energy comprising secondary electrons that had been produced by ionization of the gas.

Later Oleson and Found noticed two electron temperatures associated with moving striations.[21] The higher energy electron group was associated with the bright portion of the striation and the lower energy group with the dark region. By successive approximations, they resolved the data into two groups having distinct Maxwellian distributions. The method of successive approximations was also used later by Jones *et al.* [22] and by Scarlatto[23] from the dispersion relation of ion acoustic waves, which gave the effective temperature of the electrons in terms of the hot and cold groups, where N_0, N_c, N_H were the total, cold, and hot electron group densities, respectively. Here T_{eff} was shown to be the temperature that determined the ion acoustic speed, i.e.,

$$\frac{N_0}{T_{\text{eff}}} = \frac{N_c}{T_c} + \frac{N_H}{T_H}, \tag{27}$$

$$C_s = (KT_{\text{eff}}/M_i)^{1/2}. \tag{28}$$

Equation (27) indicates that T_{eff} is dominated by the cold group and that even a small number of cold electrons can lower the effective temperature significantly.

E. Present data

Figures 11 and 12 represent data in connection with this paper. Each figure contains three Langmuir plots, using a bare spherical probe along the chamber axis. As the focal region is approached, both figures show an increased number density due to B, the relative number density of the beam to the total density, for a relatively constant plasma potential V_p throughout the target plasma.

Poisson's equation required that the increased ion den-

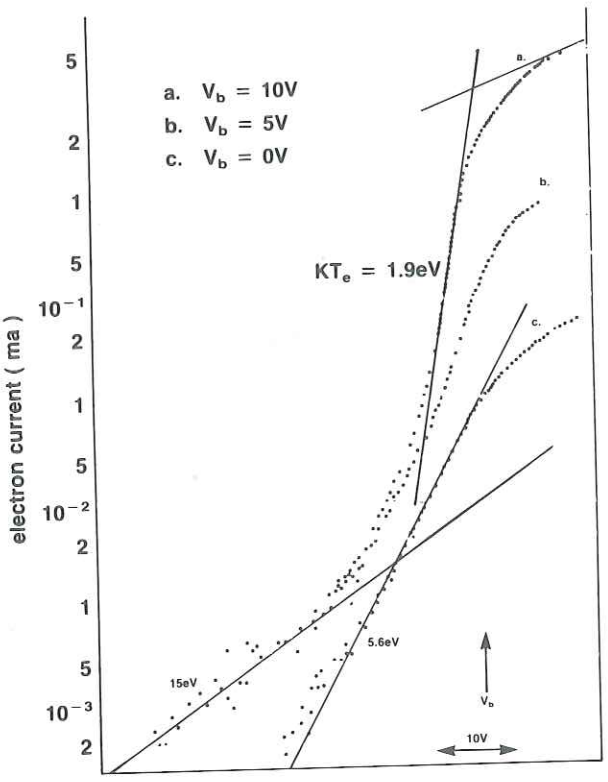

FIG. 11. Three Langmuir plots taken at the focus for various beam energies. A third, cold-temperature component occurs only in the presence of an ion beam. The hotter components are due to the primary and secondary electrons in the plasma.

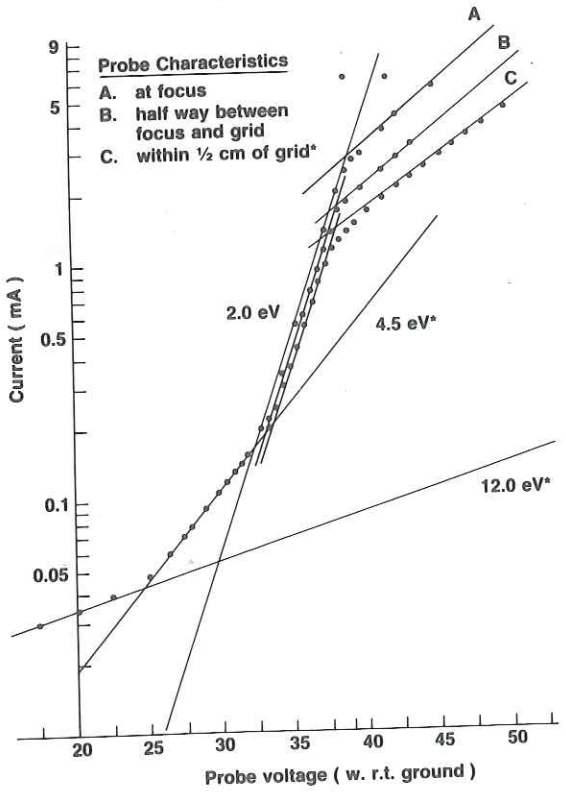

FIG. 12. Three Langmuir plots taken at various positions with a constant beam energy of 10 eV. For position *C*, the hotter electron temperature components are each reduced by one-third and the current scale has been multiplied by a factor of 10.

sity in the focal region must be neutralized by an equal increase in the electron density in order to keep the space potential of the focal region the same as that of the surrounding target plasma. This neutralization of the beam ions must be done by electrons from the target plasma since the electrons in the driver plasma are isolated from the target plasma owing to the negative potential of the hemispherical separating screen.

Figures 11 and 12 show that the target plasma electrons are composed of *three* Maxwellian components: Primary electrons coming directly from the filaments make up the hottest, most tenuous group, having an electron temperature of approximately 12 eV in Fig. 11 and 15 eV in Fig. 12. The secondary electrons coming from the ionized argon atoms make up the bulk of the target electrons, having an uncorrected temperature of 4.5 eV in Fig. 11 and 5.6 eV in Fig. 12, respectively. The temperature and density of these hotter groups depend very little upon B, whereas the density of the coldest group greatly depend on B. Neutralization of the beam ions must be accomplished, therefore, by the coldest electrons.

The exact procedure for obtaining the corrected temperature and number density for each of the three energy groups requires an extension of successive approximations to this case and is given elsewhere.[24] It yields the relation

$$\frac{1}{T_{\text{eff}}} = \left(\frac{N_p}{N_0}\right)\frac{1}{T_p} + \left(\frac{N_s}{N_0}\right)\frac{1}{T_s^*} + \left(\frac{N_t}{N_0}\right)\frac{1}{T_t^{**}} \qquad (29)$$

corresponding to the Eq. (27) for the two-electron tempera-

TABLE I. Plasma parameters in and around the focal region for a 6.5 V beam.

	5 cm in front of focus	At focus	10 cm behind focus
V_b (V)[a]	6.5	6.5	6.5
V_p (V)[b]	38	38	38
V_f (V)[c]	26	29	24
i_p (mA)	0.05	0.05	0.05
i_s (mA)	0.10	0.12	0.15
i_t (mA)	0.75	0.83	0.20
T_p (eV)	12	12	12
T_{s_*} (eV)	4.5	4.5	4.5
T_s (eV)	2.8	2.8	2.8
T_{t_*} (eV)	2.0	1.9	2.0
$T_{t_{**}}$ (eV)	1.5	1.5	1.5
T_t (eV)	0.8	0.8	0.8
$N_p/10^8$ cm^{-3}	0.11	0.11	0.11
$N_s/10^8$ cm^{-3}	0.45	0.54	0.67
$N_t/10^8$ cm^{-3}	6.29	6.96	1.68
$N_0/10^8$ cm^{-3}	6.85	7.60	2.45
N_p/N_0	0.016	0.014	0.055
N_s/N_0	0.065	0.071	0.339
N_t/N_0	0.919	0.915	0.606
T_{eff} (successive approximate) (eV)	0.85	0.85	1.13

[a] V_b is beam energy.
[b] V_p is plasma potential.
[c] V_f is floating potential.

ture case. Values of the quantities in Eq. (29) are tabulated in Table I for an ion beam energy of 6.5 V, V_f is the floating potential of the probe N_0 N_p, N_s, and N_t are the total number density, the primary number density, the secondary number density, and the tertiary number density, respectively. Here, T_p is the primary electron temperature, T_s^* is the corrected secondary electron temperature, and T_t^{**} is the corrected tertiary electron temperature. The latter two temperatures were obtained by the method of successive approximations as previously noted.

In contrast to the two-electron temperature plasma, where T_{eff} can be found using Eq. (28), the three-electron temperature case is more complex in that the ion beam modes and the ion acoustic wave are usually present simultaneously. Such a situation makes an accurate measurement of the velocity of the ion acoustic wave very difficult. As a result, Eq. (28) often cannot be used to find T_{eff} and be checked with Eq. (29). Alternately, Eq. (29) can be taken as the definition of T_{eff} and the ion acoustic velocity calculated from Eq. (28). This is the route taken here.

Figures 11 and 12 show the appearance of a low-temperature electron group in the target plasma when an ion beam is passed through the hemispherical separating screen from the driver plasma to the target plasma. This low energy group is in addition to the primary and secondary energy groups. These latter two groups remain, even in the absence of an ion beam. Table I indicates that the primary number density and electron temperature are everywhere the same. One would expect this as the primary electrons cause the plasma to form and their high energies ensure reflection by the magnetic cusps existing at the walls. On the other hand, the number density of the secondary energy group increases with decreasing distance from the target anode. Since its electron temperature is constant over this same region, the concentration of electrons in this case must increase as the target anode is approached. The presence of these two groups was detected as the two straight line segments in Figs. 11 and 12.

F. Comments on the low-energy group of electrons

Table I reveals that the low-energy group of electrons (which always make their appearance when an ion beam is sent from the driver plasma to target plasma) have a much greater number density than the accompanying primary and secondary groups, especially near the focus. Its maximum density occurs in the region of the focus and decreases sharply as the distance from the hemispherically dividing screen is increased. Figure 11 shows that the maximum number density increases with beam energy, having a peak in the neighborhood of the focus. Figure 12(c) reveals that the low-energy group has an appreciable probe current as close as 0.5 cm to the dividing grid and also retains the same electron temperature that it has at the focus. On the other hand, the densities and temperatures of the primary and secondary electron groups are considerably reduced very close to the separating grid. Without further analysis, all that can be concluded from these observations is that an ion beam coming from the driver plasma and passing through a spherical grid on to the target plasma, results in the creation of a low-energy group of electrons everywhere in the target plasma. Their number density increases with distance from the hemispherical grid, as indicated by Figs. 12(a) and 12(b), until the focal region is reached. Beyond this region, the density of these cold electrons decreases with distance, as previously discussed.

There are statistical methods of finding relaxation rates for processes resulting from the interaction of test particle streaming with a definite velocity through a background of field particles of known temperature.[25,26] In our case, the test particles are the positive ions streaming with a given velocity from the driver plasma through the hemispherical screen and the field particles are the electrons in the target plasma with a given electron temperature, presumably that of the cold electrons, with a given number density. In a less complex geometry, one could calculate such quantities as the slowing-down time and energy loss, using the observed cold temperature and number density to check the reasonableness of the results. The difficulty in the present case with a hemispherical screen is that the number density of the cold electrons is a function of the distance from the screen so straightforward calculations are not feasible.

Recall that, originally, the collector of the ion analyzer was held at -50 V to repel any high-energy electrons. This was found to be unnecessary as the plasma potential was typically 35–45 V above ground and the hottest electron group was typically 12 to 15 V.

Thus the ion current characteristics of the collector plate were found to be identical for ground potential as for -50 V. A collector plate at ground potential was still negative enough to repel most of the higher-energy electrons through the screens from the plasma, resulting in the elimination of any potential difference between the walls and the collector plate.

VI. SUMMARY AND CONCLUSIONS

(1) Three types of probes were used to monitor the target plasma in a hemispherically converging ion beam plasma system: (a) Simple Langmuir probes were used to monitor the electron temperature and density; (b) a space-charge-sensitive emissive probe was used to monitor the space potential, and (c) ion-sensitive gridded probes were used to measure the energy distribution of the plasma and beam ions.

(2) A simple theory was presented to explain the change in the probe floating potential in the presence of ion beams.

(3) The method of successive approximations, developed previously for a two-electron temperature plasma, was extended to a three-electron temperature plasma. The ion acoustic velocity is given by Eq. (28), where T_{eff} is found from Eq. (29). A full discussion of the three-electron energy case is given in Ref. 24.

(4) Attempts to use statistical methods to calculate the observed cold temperature of the electrons were not possible because of the variation of the number density with distance from the hemispherical dividing grid. Currently, the possibility of using a numerical simulation method is being considered.

ACKNOWLEDGMENTS

The referee's comments were invaluable in providing a more readable manuscript. George Pidick also deserves our thanks for serving as a troubleshooter and for maintaining the equipment in working order.

We appreciate the action of the University of South Florida for financial support on this basic research by providing funds for equipment.

APPENDIX A: COLD ION AND FINITE ION TEMPERATURE MODELS

Two models were used to explain the results of Fig. 9. The first model, Fig. 13, assumed only cold ions and four assumptions were made:

(1) All ions entered the target plasma along radii of the hemispherical separating screen.

(2) The beam *speed* U_b was constant.

(3) The ion energy analyzer collector measured velocity components normal to its surface.

(4) The ion beam density was constant everywhere on the hemispherical grid. Referring to Fig. 13: R = the radius of the hemisphere, r_p = the radius of the plane collector surface, x = the probe distance from focus, A_r = the differential area of the ring at the edge of the cap. $= 2\pi R^2 \sin\phi\, d\phi$, and A_c = the area of the hemisphere subtended by the cone formed by the collector and the focus, $A_c = 2\pi R^2 \times [1 - x(r_p^2 + x^2)^{-1/2}]$.

The calculated average kinetic energy (over ϕ) is just

$$\overline{KE} = \int_0^{\phi m} \frac{\frac{1}{2}M_i(U_b\cos\phi)^2(2\pi R^2\sin\phi\, d\phi)}{A_c = 2\pi R^2(1-X)},$$

where

$$\phi_m = \cos^{-1} X,$$

$$X = x(r_p^2 + x^2)^{-1/2},$$

and the solution is

$$\overline{KE} = \tfrac{1}{3}(\tfrac{1}{2}M_i U_b^2)(1 - X^3)/(1 - X). \qquad \text{(A1)}$$

This equation was plotted as the solid curve in Fig. 9.

Figure 14 shows the effect of a finite ion temperature.

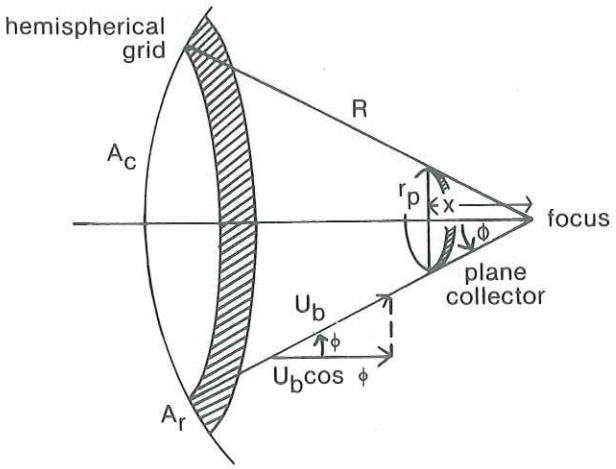

FIG. 13. Schematic of beam ions passing through hemispheric grid to ion collector located at a distance x from focus for $T_i \doteq 0$.

Beam ions enter the target plasma through an angular spread of 2θ. The collective effect of the thermal ions is to produce a focal region centered about the focal point where the ion velocity may be very complicated. For example, Fig. 8 shows a certain "filling in" of lower energies when the energy analyzer was located near the focus. The filling of lower energies due to the finite temperature of the beam ions may qualitatively explain why the measured average perpendicular energy drops off faster (except at the focus) than the expected values obtained from the model in Fig. 13, which assumes that $T_i = 0$. If the effect in Fig. 14 is included in the model in Fig. 13, the problem becomes much more complicated, but when solved, could yield better agreement between the measured and calculated values of average kinetic energy.

The radius of the focal region in Fig. 14 can be shown to be

$$a = R\,(KT_i/2eV_b)^{1/2}, \qquad \text{(A2)}$$

where R is the radius of the hemispherical grid, $eV_b = e(V_d - V_i)$ is the beam energy, and T_i is the ion tempera-

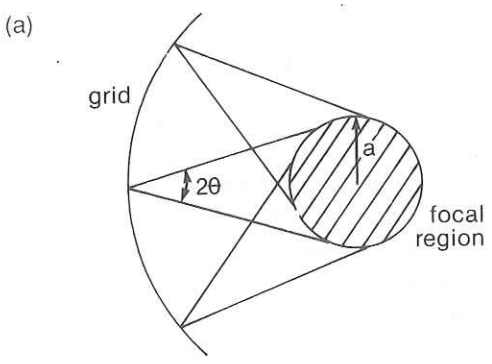

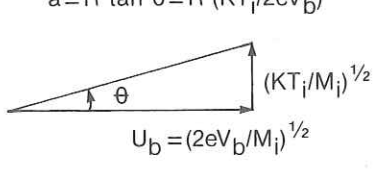

FIG. 14. Schematic of angular spread of ions as they pass through the hemispherical grid due to their finite temperature T_i.

TABLE II. Radius of focal region, a(cm) for various ion temperatures and beam energies.

KT_i (eV)	0.1	0.2	0.3
eV_b (eV)			
2	1.4	2.1	2.46
4	1.0	1.42	1.74
6	0.82	1.16	1.42
8	0.71	1.01	1.23
10	0.64	0.90	1.10

ture. Values of a(cm) for different beam energies and ionic temperatures are given in Table II.

APPENDIX B: DETERMINATION OF B AT THE FOCUS

Figure 6 shows the method used to determine B at a point well behind the focus. The method is quite clear owing to the distinctness of the two ion groups there. The question arises as to how to interpret the ion current characteristics taken at the focus.

Figure 15 is the ion characteristic at the focus, taken from Fig. 5. Two methods are depicted for determining the

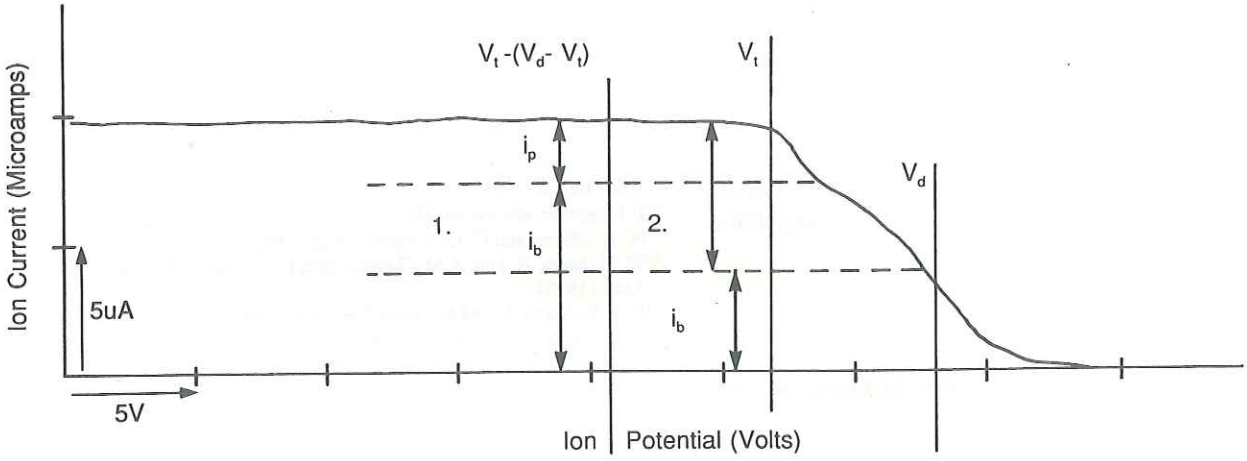

FIG. 15. Determination of B from methods (1) and (2) (see Appendix B).

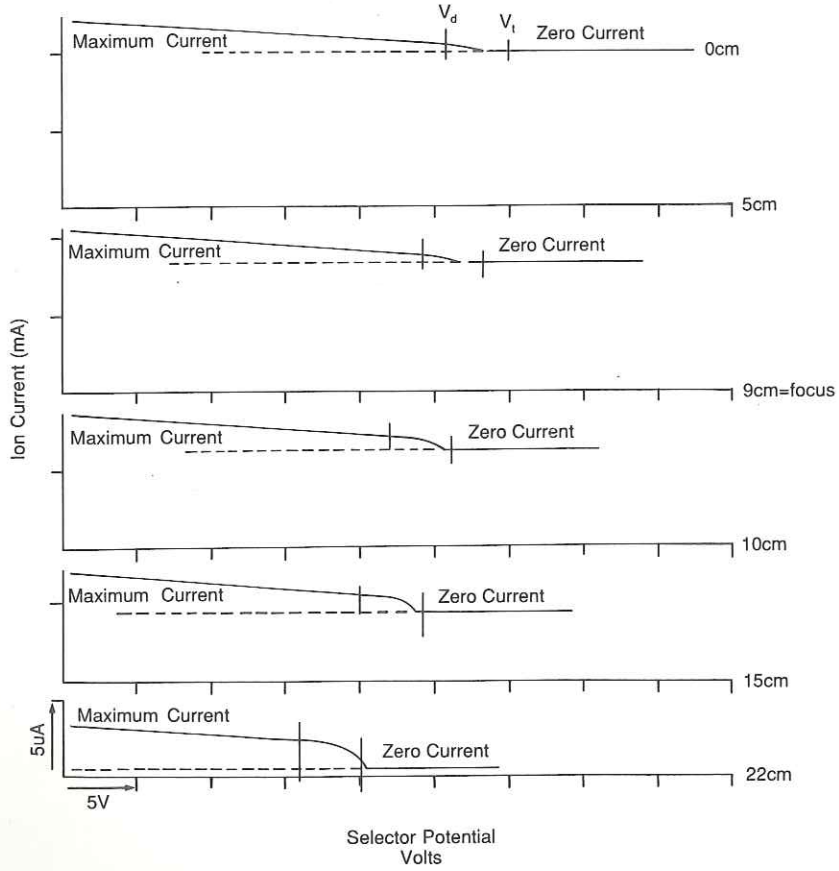

FIG. 16. Ion collector currents versus selector grid voltage for V_d less than V_t.

values of i_p and i_b used in Eq. (13) for B. In the first method, the dotted line is drawn from the "crook" in the characteristic. This means, from Fig. 5, that the *target* plasma is more dense close to the filaments (see Fig. 1) and less dense at the focus. Method (2) assumes first off that i_p is a special invariant and that any "leftover" current is the current due to the beam ions i_b. Method (1) gives $B = 95\%$ at the focus and $B = 18\%$, 10 cm behind the focus. Method (2) gives $B = 48\%$ at the focus and $B = 1\%$, 10 cm behind the focus. Both methods indicate that the focal region is one of higher B.

The assumption made in method (2) (that i_p is everywhere the same) does not seem to be realizable. Figure 16 depicts a series of ion current characteristics taken at different points along the axis of the plasma, similar to Fig. 5, only this time the driver plasma was set at a voltage that was *less* than the target plasma to ensure the *absence* of any beam ions in the target plasma. This figure clearly shows a diminishing ion saturation current at points farthest from the test plasma filaments, including the focal region. Thus it would seem to favor method (1) over method (2), meaning that B could be as high as 95% in the focal region.

[1]R. J. Taylor, K. R. MacKenzie, and H. Ikezi, Rev. Sci. Instrum. **43**, 1675 (1972).
[2]T. Honzawa, Phys. Fluids **27**, 1013 (1984).
[3]E. G. Zaidman and N. L. Oleson, IEEE Trans. Plasma Sci. **PS-17**, 24 (1989).
[4]H. Akiyama, T. Yamada, and S. Takeda, Jpn. J. Appl. Phys. **18**, 1543 (1979).
[5]Y. Nakamura and T. Ogino, Plasma Phys. **24**, 1295 (1982).
[6]T. Honzawa, Plasma Phys. Controlled Fusion **26**, 449 (1984).
[7]T. Honzawa, Phys. Rev. Lett. **53**, 1915 (1984).
[8]T. Honzawa and M. Kuroda, Phys. Fluids **29**, 3052 (1986).
[9]I. Mori and K. Ohya, Phys. Rev. Lett. **59**, 1825 (1987).
[10]C. Chan, T. Intrator, and N. Hershkowitz, Phys. Lett. A **91**, 167 (1982).
[11]M.-H. Cho, N. Hershkowitz, and T. Intrator, J. Appl. Phys. **67**, 3254 (1990).
[12]C. Mattson, M. S. thesis, University of South Florida, 1976.
[13]C. E. Garner, M.S. thesis, University of South Florida, 1982; C. E. Garner and N. L. Oleson, Bull. Am. Phys. Soc. **34**, 2130 (1989).
[14]J. D. Swift and M. J. R. Schwar, in *Electrical Probes for Plasma Diagnostics* (American Elsevier, New York, 1969).
[15]J. R. Smith, N. Hershkowitz, and F. Coakley, Rev. Sci. Instrum. **50**, 210 (1979).
[16]H. Ikezi and R. J. Taylor, Phys. Rev. Lett. **22**, 923 (1969).
[17]T. Romesser and N. Hershkowitz, Phys. Fluids **18**, 1354 (1975).
[18]N. Hershkowitz, in *Plasma Diagnostic Techniques* (Academic, New York, 1989), pp. 113–183.
[19]J. D. Lawson, *The Physics of Charged Particle Beams*, 2nd ed. (Clarendon, Oxford, 1988), Chap. 6.
[20]I. Langmuir and H. M. Mott-Smith, Phys. Rev. **28**, 4 (1926).
[21]N. L. Oleson and C. G. Found, J. Appl. Phys. **20**, 416 (1949).
[22]W. D. Jones, A. Lee, S. M. Gleman, and H. J. Doucet, Phys. Rev. Lett. **35**, 1349 (1975).
[23]P. P. Scarlato, Jr., M.S. thesis, University of South Florida, 1977.
[24]J. M. Peterson and N. L. Oleson, IEEE Trans. Plasma Sci. **PS-19**, 419 (1991).
[25]B. A. Trubinow, Rev. Plasma Phys. **1**, 105 (1965).
[26]D. L. Book, *NRL Plasma Formulary* (U.S. GPO, Washington, DC, 1990).